Available online at www.sciencedirect.com
ScienceDirect
Ceramics International 37 (2011) 2229–2236
CERAMICS INTERNATIONAL
www.elsevier.com/locate/ceramint

Synthesis of $La_{1-x}Sr_xMnO_3$ powders by polymerizable complex method: Evaluation of structural, morphological and electrical properties

Leandro da Conceição, Nielson F.P. Ribeiro, Mariana M.V.M. Souza *

Escola de Química – UFRJ, Centro de Tecnologia, Bloco E, Sala 206, CEP 21941-909, Rio de Janeiro, RJ, Brazil

Received 8 September 2010; received in revised form 30 December 2010; accepted 7 March 2011
Available online 14 April 2011

Abstract

Lanthanum strontium manganite ($La_{1-x}Sr_xMnO_3$, LSM) powders were synthesized by polymerizable complex method, based on complexation of metal ions (MI) with citric acid (CA) and polyesterification between CA and ethylene glycol (EG). Firstly, the effect of the molar ratio of CA:MI (=1–3) was investigated on the synthesis of $La_{0.7}Sr_{0.3}MnO_3$ powders, which were characterized by thermal analysis (TGA/DTA), X-ray diffraction (XRD), and scanning electron microscopy (SEM). The results indicated that the molar ratio CA:MI = 3 is adequate for a good crystallization of pure perovskite phase after calcination, with nanometric crystallite sizes and porous microstructure. For the $La_{0.7}Sr_{0.3}MnO_3$ sample synthesized with CA:MI ratio of 3, it was investigated the effect of calcination temperature, showing that the perovskite structure is better crystallized at 900 °C, without secondary phase formation. Using this same CA:MI ratio and calcination temperature, powders with different Sr content (x = 0.2–0.4) were synthesized, with surface areas of 4–10 $m^2\ g^{-1}$. These powders were sintered at 1100 °C to produce porous pellets. The porosity of the sintered pellets and the electrical conductivity, measured by two-probe technique, increased with increasing Sr content.

Keywords: A. Powders: chemical preparation; B. X-ray methods; C. Electrical conductivity; D. Perovskites; Lanthanum strontium manganite

1. Introduction

Solid oxide fuel cells (SOFCs) have become of great interest as a potential economical, clean and efficient means of producing electricity in a variety of commercial and industrial applications [1]. Lanthanum strontium manganite (LSM) is known to be a potential cathode material for SOFCs based on stabilized zirconia electrolyte because of its high electrical conductivity, chemical and thermal stability, high catalytic activity for the oxygen reduction and its compatibility with zirconia electrolyte [1,2]. The cathode material should have porosity between 20 and 40% and an electrical conductivity higher than 100 S cm^{-1} (measured by four-probe method) [3]. The crystalline structure of LSM depends on Sr-doping degree, in general it is rhombohedral, although some authors observed that LSM structure became cubic for $x > 0.3$, as shown by Gaudon et al. [4].

Recently, much attention has been given on the preparation method as the actual composition and properties of the materials depend on the synthesis procedure. The homogeneous starting powder is a prerequisite for the manufacturing of high performance electrodes, since the microstructure and properties of ceramics are significantly influenced by the characteristics of preliminary powder. Thus, it is fundamental to prepare high-quality powders with controlled stoichiometry and microstructure.

Several synthesis methods have been developed for preparation of LSM powders, such as solid-state reaction [5], combustion method [6,7] and some solution chemistry methods, for example, sol–gel process [4], co-precipitation technique [8] and citrate process [9–11]. Particularly, solution chemistry methods are used to prepare materials of high purity, with small grain size and at lower temperature compared to the conventional solid-state method [12].

The polymerizable complex method, developed by Pechini [13], uses citric acid (CA) to chelate metal ions (MI) and ethylene glycol (EG) as a solvent for the process of polymerization to form an intermediate of polyester-type resin. According to Popa and Kakihana [14] the process consists of

* Corresponding author. Tel.: +55 21 25627598; fax: +55 21 25627596.
E-mail address: mmattos@eq.ufrj.br (M.M.V.M. Souza).

0272-8842/$36.00
doi:10.1016/j.ceramint.2011.03.069

three major steps: (i) complexation of metal ions with citric acid in water; (ii) polymerization, where the formed chelates undergo polyesterification with ethylene glycol; and (iii) decomposition of the organic network to obtain the powder precursor.

It is well known that the ratios of the reactants and the conditions of the polyesterification have a considerable influence on the purity and properties of the final product [9–11,14]. Yang et al. [10] investigated the effect of CA:MI molar ratio on the synthesis of $La_{0.67}Sr_{0.33}MnO_3$ powders by polymerizable complex process, showing that with the ratio of 4 the powder exhibited a pure phase of perovskite, with nanometric particle size and high specific surface area. According to Gaki et al. [11] the molar ratio CA:MI = 2 is the most favorable for the synthesis of $LaMnO_3$. Thus, the optimum CA:MI ratio for synthesis of LSM is not well established in the literature.

In the present study we have attempted to optimize the synthesis conditions of LSM powders by polymerizable complex method, searching the minimum molar ratio of CA:MI and calcination temperature to obtain pure crystalline phase of perovskite with nanometric sizes. Different ratios were used for the synthesis of $La_{0.7}Sr_{0.3}MnO_3$ and the optimal value obtained was applied to synthesize $La_{1-x}Sr_xMnO_3$ with $x = 0.2$–0.4, whose structural, morphological, and electrical properties were investigated.

2. Experimental

2.1. LSM preparation

The starting materials used in this study were metal nitrates ($La(NO_3)_3{\cdot}6H_2O$, $Sr(NO_3)_2$ and $Mn(NO_3)_3{\cdot}4H_2O$), ethylene glycol ($C_2H_6O_2$) and citric acid ($C_6H_8O_7$). All reagents were from Vetec (Brazil) with 99.0% of purity. $La_{1-x}Sr_xMnO_3$ powder materials were prepared in the primary study with nominal composition of $x = 0.3$, and then Sr composition was varied between $x = 0.2$ and 0.4.

The metal nitrates in the required stoichiometric ratio were dissolved in deionized water together with citric acid (CA:MI molar ratios of 1, 2 or 3) and ethylene glycol (EG) (1:1, EG:CA). The solution was heated at 60 °C for homogenization and then the temperature was increased to 110 °C in oil bath under constant stirring for 24 h to eliminate the excess water and accelerate the polyesterification reaction between CA and EG. As the polymerization reaction proceeded, a homogeneous sol was obtained and further heated at 110 °C in an oven for 8 h to remove the excess of solvent, forming an intermediate resin. The resin was calcined at 750 °C in the primary study and then at 900 °C, for 10 h in flowing air.

The powders were uniaxially pressed at 280 MPa and the green pellets were sintered at 1100 °C for 4 h with a heating rate of 10 °C min^{-1}. The sintering temperature was chosen based on the results of Li et al. [15], although they had used gelcasting for preparing LSM cathode materials. This is a preliminary choice; of course, it is important to study different sintering temperature to produce materials with proper surface area and porosity. In this study, we evaluated the potential of these materials to be used as cathode for SOFC, we did not optimize the sintering temperature.

2.2. Characterization

Thermogravimetric analysis (TGA) and differential thermal analysis (DTA) of the as-prepared powders were carried out using a TA thermal analyzer (SDT Q600 model), with a heating rate of 5 °C min^{-1} from room temperature to 1300 °C in air.

The prepared powders were analyzed by powder X-ray diffraction (XRD), in a Rigaku Miniflex II diffractometer with monochromator, using CuKα radiation (λ = 1.54055 Å), with a step size of 0.05°, speed of 2° min^{-1} and over the 2θ range of 5° and 90°. The crystallite sizes (D_{XRD}) and microstrain (ε) were calculated using the model proposed by Williamson and Hall [16], by means of the following formula:

$$\frac{\beta\cos\theta}{\lambda} = \frac{1}{D_{XRD}} + 4\varepsilon\frac{\sin\theta}{\lambda} \quad (1)$$

where θ is the diffraction angle, λ is the wavelength of incident radiation and β is the full width at half maximum (FWHM) of the peak. Plotting the $\beta\cos\theta/\lambda$ versus $4\sin\theta/\lambda$ straight line yields the crystallite size from interception with the ordinate and microstrain from the slope.

The microstructure of LSM powders was investigated by scanning electron microscopy (SEM) using Hitachi TM-1000 equipment. The acceleration voltage was 15 kV, using back-scattering electron.

Textural analysis was performed by physical adsorption of N_2 (BET method) with a Micromeritics ASAP 2000 equipment. Prior to analysis, the samples were outgassed for 24 h at 300 °C. The average particle size (D_{BET}) was calculated assuming the presence of spherical particles, by means of the equation:

$$D_{BET} = \frac{6}{\rho_t S_{BET}} \quad (2)$$

where ρ_t is the theoretical density of LSM (6.45 g cm^{-3} for $La_{0.7}Sr_{0.3}MnO_3$) and S_{BET} is the specific surface area. The apparent densities of the LSM pellets were determined by the Archimedes method using water. The porosity of the pellets was calculated by the equation:

$$P = \frac{\rho_t - \rho_A}{\rho_t} \times 100 \quad (3)$$

where P is the porosity (%), ρ_t is the theoretical density (g cm^{-3}) and ρ_A is the apparent density (g cm^{-3}).

Electrical conductivity of sintered porous bodies was measured by DC two-probe technique, with a HP 34420A multimeter, using platinum electrodes in a thermoelectric furnace MAITEC, at temperature range of 500–1000 °C. Pt paste was painted on the surface of the sintered pellet. The conductivity (σ) of the samples was calculated by measuring the resistance (R) between the two electrodes and knowing the

values of the thickness (L) and the surface area (S) of the pellet:

$$\sigma = \frac{L}{RS} \quad (4)$$

The average thickness was 1.5 mm and the surface area was 1.25 cm^2.

3. Results and discussion

3.1. The influence of CA:MI molar ratio and calcination temperature

3.1.1. Thermal analysis

The TGA/DTA curves of the as-synthesized LSM powders, prepared with different CA:MI molar ratios, are displayed in Fig. 1. The TGA profiles presented three decomposition stages. The first stage, from 50 to 250 °C, is attributed to the loss of water and volatile organic species. The second stage, from 250 to 550 °C, responsible for the major weight loss, is associated with the decomposition of polymer network with possible formation of carbonates and burnout of most of the organic residues [10,11]. At this stage, there is decomposition of nitrates with formation of NO_x [17]. The weight loss in the second stage increases as CA:MI ratio increases indicating a larger formation of polymer network. The third stage, above 550 °C, is related to decomposition of carbonate species [18,19], as will be confirmed by XRD analysis in function of calcination temperature. Although the work of Gaoke et al. [19] deals with preparation of $SrCoO_3$, they observed the same formation of $SrCO_3$ phase by polymerized complex method, as we did by XRD.

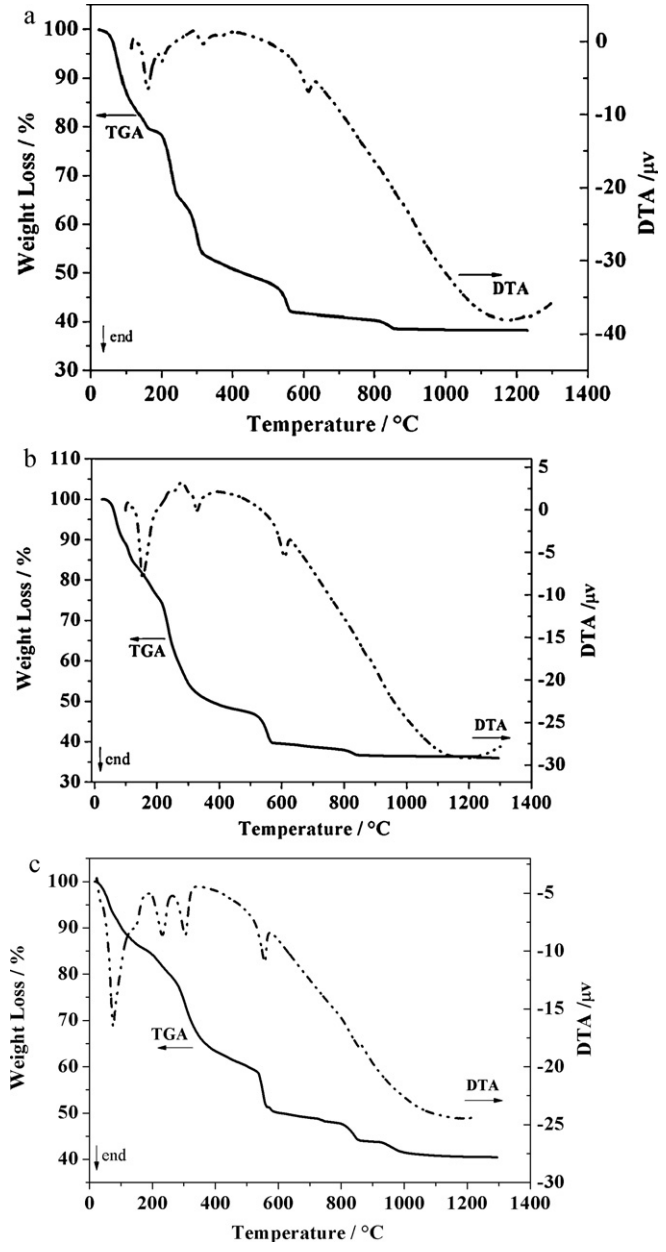

Fig. 1. TGA and DTA curves of the as-synthesized $La_{0.7}Sr_{0.3}MnO_3$ powders, prepared with CA:MI ratio of 1 (a), 2 (b) and 3 (c).

The DTA curves show four endothermic peaks. The first two peaks, observed below 250 °C, are related to evaporation of moisture and low boiling organic species. A third peak at approximately 300 °C is associated with the decomposition of polymer network, and the fourth peak at about 560 °C is due to carbonate decomposition [19].

Metal nitrates and organics, like citric acid (CA), can be used in combustion synthesis of perovskites, in this case the mixture is heated until it ignites. In the case of polymerizable complex method there is formation of a stable metal–chelate complex between metal nitrates and CA and then a polymeric resin is formed in the presence of ethylene glycol (EG). The metal cations are homogeneously distributed in the polymeric resin and no combustion is observed. This can be confirmed by DTA analysis since no exothermic peak due to combustion was observed.

3.1.2. Phase formation

Fig. 2 shows the XRD patterns of the LSM powder samples prepared with different CA:MI ratios after calcination. The sample prepared with CA:MI ratio of 1 exhibited a mixture of phases, which were not identified. This result shows that it is difficult to maintain the homogeneity of the metal ions in the resin on a molecular scale when the ratio of CA:MI is low. The low concentration of CA prevents a good polymer matrix formation and consequently poor crystalline structures are obtained after calcination, as observed in previous studies [10,11].

The sample prepared with CA:MI ratio of 2 presented a great improvement in the phase formation, without secondary phases, but LSM is still poorly crystallized. XRD pattern of the sample synthesized with CA:MI ratio of 3 shows only the presence of $La_{0.7}Sr_{0.3}MnO_3$ phase (ICSD 473444) with high crystallinity. Thus, the minimum CA:MI ratio necessary for a proper formation of the polymer matrix and a good crystallization of perovskite phase after calcination is 3. This value is close to that obtained by Yang et al. [10], who observed that with molar ratio of CA:MI at 4, the resin contained a higher portion of C–C–O structure from EG, which made it possible to synthesize a pure phase of LSM at calcination temperature of 500 °C.

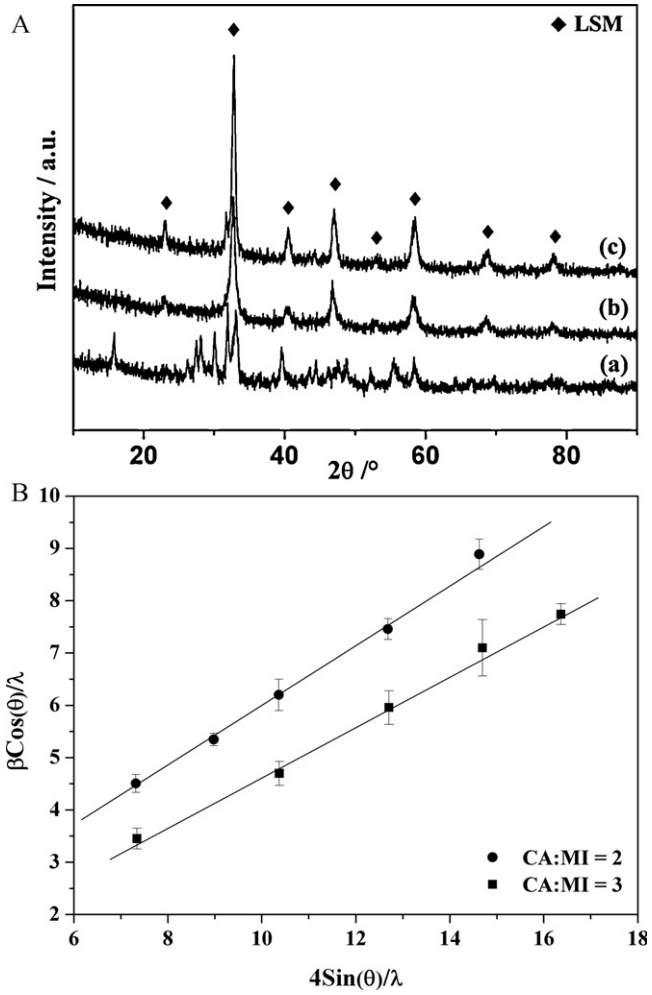

Fig. 2. (A) XRD patterns of $La_{0.7}Sr_{0.3}MnO_3$ powders prepared with CA:MI ratio of 1 (a), 2 (b) and 3 (c), after calcination at 750 °C for 10 h, and the corresponding Williamson–Hall plots (B).

Gaki et al. [11], when synthesizing $LaCoO_3$, also observed that some precipitation occurred with solutions containing CA:MI ratio of 1, affecting the homogeneity of the final product, with formation of several secondary crystalline phases. They concluded that the molar ratios CA:MI = 2 and EG:CA = 3 were the most favorable for the synthesis of $LaMO_3$ (M=Mn, Co or Fe).

The average crystallite sizes and microstrain of LSM powders prepared with different CA:MI ratios and the lattice parameters of the perovskite structure are shown in Table 1. The data for LSM sample prepared with CA:MI ratio of 1 cannot be calculated because of the large number of phases that were

Table 1
Average crystallite size (D_{XRD}), microstrain (ε) and lattice parameters of $La_{0.7}Sr_{0.3}MnO_3$ samples prepared with different CA:MI ratio.

CA:MI ratio	D_{XRD} (nm)	ε (%)	Lattice parameters (Å)
2	16.6	0.67	a = 5.4635 c = 13.4167
3	12.3	0.50	a = 5.4854 c = 13.3975

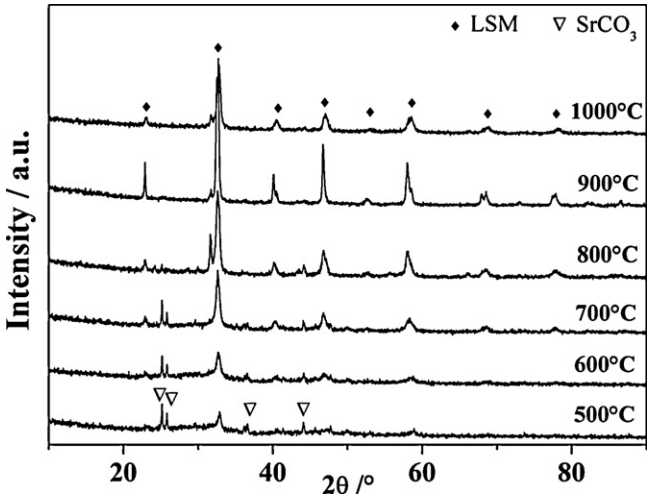

Fig. 3. XRD patterns of $La_{0.7}Sr_{0.3}MnO_3$ powders prepared with CA:MI ratio of 3 after calcination at different temperatures.

observed in its XRD pattern (Fig. 2). Both samples, with CA:MI ratio of 2 and 3, are nanocrystalline with sizes of 16.6 and 12.3 nm, respectively, and presented rhombohedral structure with lattice parameters close to those of ICSD 473444 (a = 5.4953 Å and c = 13.3422 Å).

The good straight line of the Williamson–Hall plot (Fig. 2B) suggests that the synthesis yields homogeneous materials with uniform shape because the crystallite sizes are quite similar for most crystallographic planes. The sample prepared with the highest CA:MI ratio presented smaller crystallite size and lower value of microstrain, showing that a sufficient amount of CA is necessary to maintain the homogeneity of metal ions in the resin on a molecular scale, forming small crystallites without significant lattice distortions.

Once defined the optimal value of CA:MI ratio for the synthesis of LSM, we studied the influence of calcination temperature on the phase formation. The LSM precursor prepared with CA:MI ratio of 3 was separated into equal parts and calcined at temperatures between 500 and 1000 °C in air flow for 4 h. XRD patterns of the samples calcined at different temperatures are shown in Fig. 3.

After calcination at 500 °C, the sample presents formation of $SrCO_3$, besides LSM of low crystallinity. As the calcination temperature increases, $SrCO_3$ reacts with the formed perovskite into a pure LSM structure. Carbonate phase can be observed at XRD pattern until calcination at 800 °C. These results are in accordance with TGA profiles (Fig. 1), which showed decomposition of carbonate species in temperature range of 550–800 °C. The peaks due to perovskite phase become sharper as the calcination temperature increases from 700 to 900 °C, indicating an increase in the long-range order of the perovskite lattice. However, after calcination at 1000 °C, the crystallinity decreases.

Kakihana et al. [9] and Popa et al. [20] observed a complete crystallization of $LaMnO_3$ prepared by Pechini method at 700 °C, with a monophase perovskite formation after calcination at 900 °C. On the other hand, a lot of other phases (SrO,

Table 2
Average crystallite size (D_{XRD}), microstrain (ε) and lattice parameters of $La_{0.7}Sr_{0.3}MnO_3$ samples prepared with CA:MI ratio of 3 and calcined at different temperatures.

Calcination temperature (°C)	D_{XRD} (nm)	ε (%)	Lattice parameters (Å)
700	15.7	0.40	a = 5.4853 c = 13.4655
800	21.0	0.53	a = 5.5005 c = 13.4218
900	30.0	0.68	a = 5.4985 c = 13.4218
1000	30.6	0.66	a = 5.4977 c = 13.4163

La_2O_3 and Mn_3O_4) were observed by Yang et al. [10] for LSM synthesized with CA:MI ratio of 4 and calcined at 900 °C.

The average crystallite sizes, microstrain and lattice parameters of the LSM samples calcined at different temperatures are listed in Table 2. The crystallite size increases with increasing calcination temperature until 900 °C, showing crystal growth due to sintering. Also the microstrain increases with temperature, which suggests that crystal lattice distortion due to internal stresses become more severe with heat treatment. The crystallite sizes obtained in this study are much smaller than those reported by Yang et al. [10] for LSM sample prepared from molar ratio of CA:MI at 4: 43 nm after calcination at 600 °C and 64 nm after calcination at 800 °C.

3.1.3. Microstructure

The morphology of the particles in ceramic materials is a consequence of the preparation method, and wet chemical methods favor obtaining porous nanoparticles, because the reactions produce homogeneous materials composed of small and uniform particles.

Fig. 4 shows the microstructure of LSM powders prepared with different CA:MI ratios and calcined at 900 °C for 10 h. It is interesting to note that the CA:MI ratio has a significant influence on the morphology of calcined powders. The sample prepared with deficiency of the chelating agent (CA:MI = 1) presented formation of agglomerates of fine primary particles, with low porosity. The micrograph confirmed the results discussed in the previous section, showing that the low concentration of CA prevents a good polymer matrix formation, with crystallite aggregation when the material is calcined.

There was a small improvement in the microstructure for the sample prepared with CA:MI ratio of 2, with a more loose and porous structure. When the CA:MI ratio increases to 3, the calcined powder has a spongy aspect, with formation of fine particles and a great increase in the porosity.

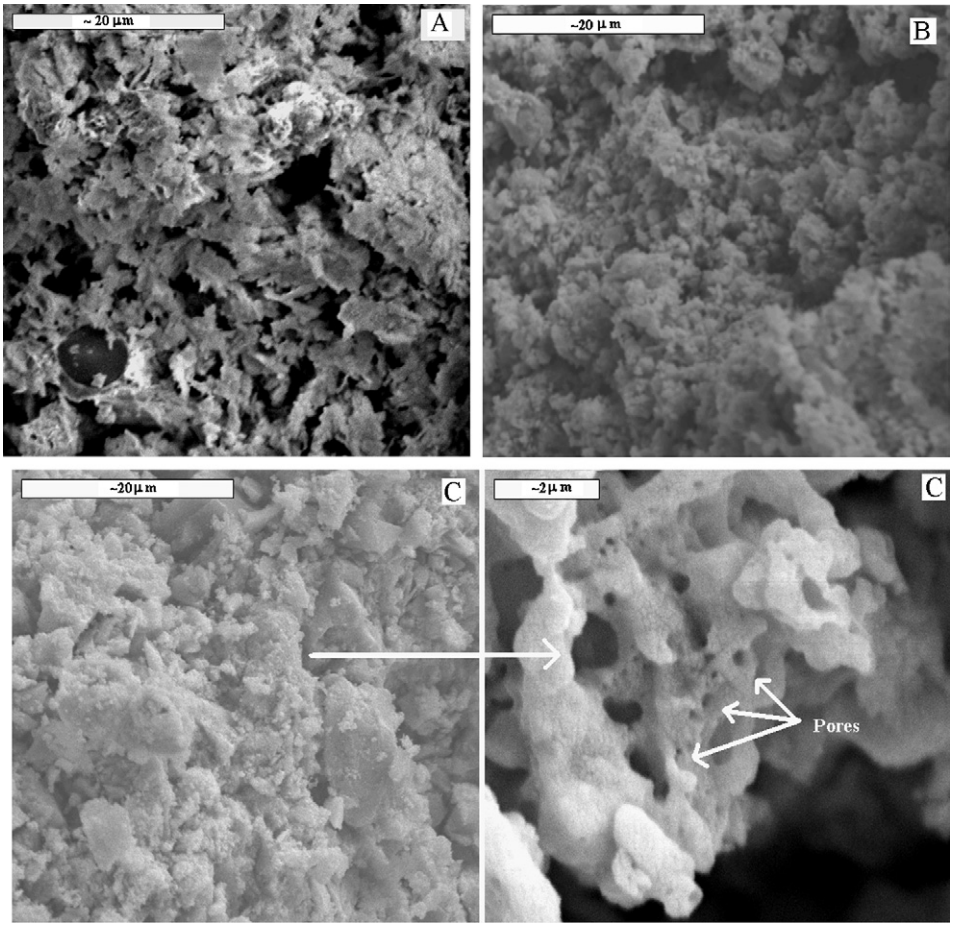

Fig. 4. Micrographs of $La_{0.7}Sr_{0.3}MnO_3$ powders prepared with CA:MI ratio of 1 (A), 2 (B) and 3 (C).

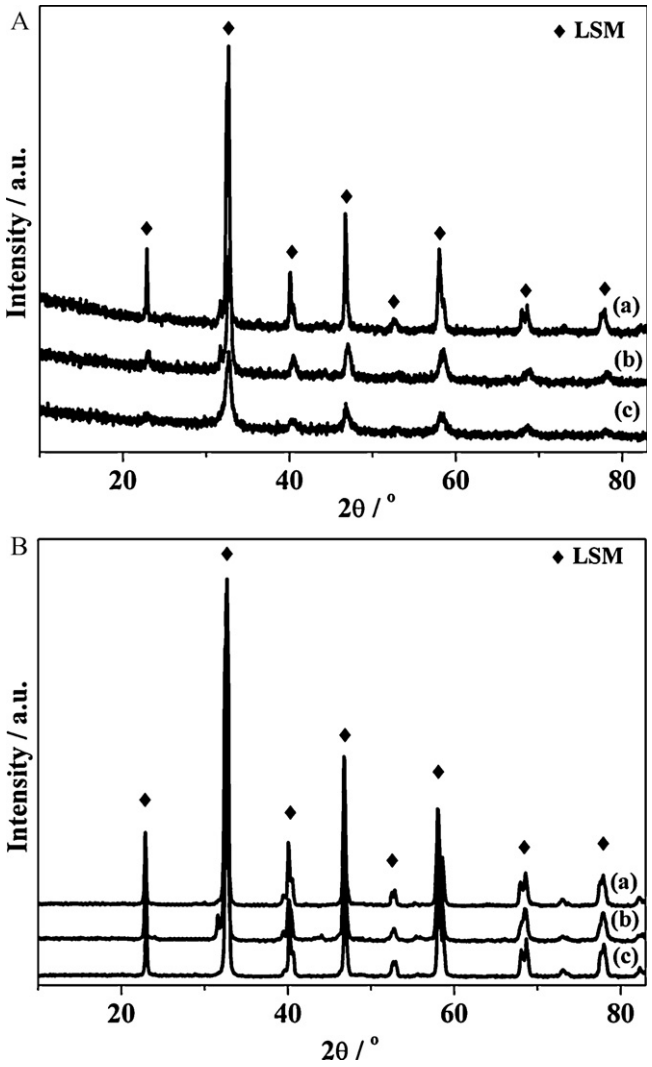

Fig. 5. XRD patterns of (a) $La_{0.8}Sr_{0.2}MnO_3$, (b) $La_{0.7}Sr_{0.3}MnO_3$ and (c) $La_{0.6}Sr_{0.4}MnO_3$ samples prepared with CA:MI ratio of 3 after calcination at 900 °C for 10 h (A) and sintering at 1100 °C for 4 h (B).

3.2. The influence of strontium content

3.2.1. Phase formation

Based on the above results of the ideal CA:MI ratio and calcination temperature for the synthesis of $La_{0.7}Sr_{0.3}MnO_3$ powders, we synthesized LSM samples with different compositions of Sr. XRD patterns of $La_{1-x}Sr_xMnO_3$ samples ($x = 0.2$; 0.3 and 0.4) prepared with CA:MI ratio of 3 and calcined at 900 °C for 10 h are shown in Fig. 5A. For all samples there was only formation of LSM phase (ICSD 473817 for $x = 0.2$, 473444 for $x = 0.3$ and 470921 for $x = 0.4$) with a significant broadening of the peaks with increasing Sr content. After sintering at 1100 °C, the XRD patterns (Fig. 5B) showed formation of sharp LSM peaks for all samples, without segregation of additional phases.

Table 3 shows the average crystallite sizes, microstrain and lattice parameters of the LSM samples with different Sr compositions, after calcination and sintering. The crystallite sizes are similar for all three samples, with only a small decrease with increasing Sr content, while microstrain increases, showing that Sr doping causes a greater number of imperfections within the crystalline lattice. The crystallite sizes increase after sintering and microstrain decreases significantly, showing a stress relaxation with temperature.

The lattice parameter c increases with Sr content due to the bigger ionic radius of Sr^{2+} (1.54 Å) as compared to La^{3+} (1.46 Å). The small decrease of parameter a with Sr content could be explained by the presence of a part of Mn ions in tetravalent state with smaller ionic radius ($r_{Mn^{4+}} = 0.53$ Å, $r_{Mn^{3+}} = 0.65$ Å in octahedral coordination) as a result of electric charge compensation, in accordance with Berger et al. [21]. The rhombohedral perovskite structure is maintained despite the increase in Sr content, which differs from the results of Gaudon et al. [4], who observed that LSM structure became cubic for $x > 0.3$.

3.2.2. Surface area and porosity

Table 4 shows the values of the surface area, pore volume and average particle size of the LSM powders with different Sr content. The BET surface areas fall in the range of 4–9.8 $m^2\ g^{-1}$, increasing with Sr content, in accordance with the results of Gaudon et al. [4]. Kakihana et al. [9] synthesized $LaMnO_3$ powders by Pechini method with surface area of 20.2 $m^2\ g^{-1}$ after calcination at 700 °C and Yang et al. [10] showed that surface areas decreased from 25.2 to 10.2 $m^2\ g^{-1}$ when calcination temperature increased from 550 to 800 °C, for LSM samples prepared with CA:MI ratio of 4.

The porosity of the LSM pellets sintered at 1100 °C is also presented in Table 4. Relative densities are strongly dependent on the sintering temperature. Li et al. [15] showed that the open

Table 3
Average crystallite size (D_{XRD}), microstrain (ε) and lattice parameters of LSM samples prepared with different Sr content, after calcination at 900 °C and sintering at 1100 °C.

Sample	D_{XRD} (nm)		ε (%)		Lattice parameters (Å)	
	900 °C	1100 °C	900 °C	1100 °C	900 °C	1100 °C
$La_{0.8}Sr_{0.2}MnO_3$	21.8	27.9	0.25	0.10	$a = 5.5182$ $c = 13.3492$	$a = 5.5254$ $c = 13.3511$
$La_{0.7}Sr_{0.3}MnO_3$	20.4	26.7	0.30	0.11	$a = 5.5145$ $c = 13.3579$	$a = 5.5223$ $c = 13.3601$
$La_{0.6}Sr_{0.4}MnO_3$	19.0	26.0	0.40	0.15	$a = 5.5050$ $c = 13.3741$	$a = 5.5182$ $c = 13.3792$

Table 4
Specific surface area (S_{BET}), pore volume (V_{pore}) and average particle size (D_{BET}) of LSM powders and apparent density and porosity of the pellets.

Samples	S_{BET} ($m^2\ g^{-1}$)	V_{pore} ($cm^3\ g^{-1}$)	D_{BET} (μm)	Apparent density ($g\ cm^{-3}$)[a]	Porosity (%)
$La_{0.8}Sr_{0.2}MnO_3$	4.7	0.021	0.19	3.9	40.1
$La_{0.7}Sr_{0.3}MnO_3$	5.3	0.035	0.17	3.4	47.2
$La_{0.6}Sr_{0.4}MnO_3$	9.8	0.038	0.09	3.0	52.5

[a] Determined by Archimedes method.

porosity decreased from 40 to 3.2% when sintering temperature increased from 1000 to 1200 °C, concluding that a proper porosity (26%) was obtained with sintering temperature of 1100 °C, as used here. The porosity increased with increasing Sr content, in the range of 40–52%, which is higher than the ideal value (20–40%) for use as cathode in SOFCs [1,3,15].

3.2.3. Electrical conductivity

$LaMnO_3$ has intrinsic p-type conductivity due to the formation of cation vacancies and the electrical conductivity of the material can be enhanced by substituting a lower-valence ion, such as Sr^{2+}, on La^{3+} sites [15]. Sr-doping enhances the electrical conductivity of $LaMnO_3$ by promoting the formation of Mn^{4+} in order to maintain local charge balance [7].

Fig. 6 shows the conductivities of the samples with different Sr content and sintered at 1100 °C as a function of temperature. The conductivities increase with temperature, as expected in a semiconducting behavior. The Arrhenius plots of $\ln(\sigma T)$ versus $1/T$ of all samples exhibit a linear dependence over a wide range of temperatures (500–1000 °C), as predicated by the following equation:

$$\ln(\sigma T) = \ln A - \frac{E_a}{RT} \quad (4a)$$

where σ, A, T, R and E_a, are respectively the conductivity of the material, a constant associated with crystalline structure and composition of material, absolute temperature, gas constant, and activation energy of conductance. The linear dependence indicates that the conductivity mechanism is by thermally activated hopping of small polarons between localized states corresponding to Mn sites of different valence [22,23]. The charge carriers are transported by the Mn^{3+}–O–Mn^{4+} network [22].

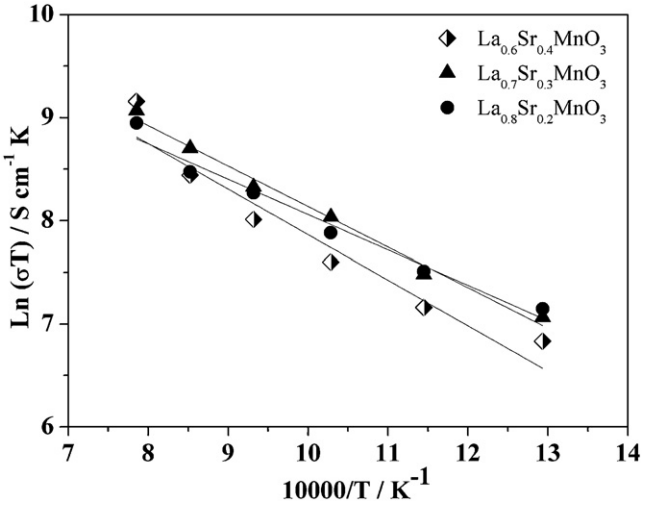

Fig. 6. The electrical conductivity of LSM pellets with different Sr content as a function of reciprocal absolute temperature.

Table 5 shows the conductivity of the samples at 600 and 1000 °C and activation energies calculated from the slopes of the Arrhenius plots. The conductivity at 1000 °C increases with increasing Sr content, which can be correlated to an increase of the formation of Mn^{4+} species in the Mn^{3+} matrix, as observed by Gaudon et al. [4]. Thus, this effect is predominant over the densification of the samples, since the porosity increased with Sr content (Table 4). The sample with higher Sr content ($x = 0.4$) presented higher value of activation energy for charge carrier hopping, that may indicate more lattice distortion since changes in the M–O–M bonds reduce charge carrier mobility between the two metal sites.

The values of conductivities in this study are very close to that reported by Yang et al. [24] for LSM sintered at 1400 °C (3.5 S cm^{-1} at 1000 °C), also using two-point probe method for conductivity measurement. However, these values are much lower than those measured by other authors using four-probe method. Guo et al. [25] reported an electrical conductivity of 150 S cm^{-1} at 800 °C for LSM sample sintered at 1300 °C. Kumar et al. [23] measured electrical conductivities of 136–146 S cm^{-1} at 1000 °C for porous $La_{0.84}Sr_{0.16}MnO_3$ sintered at 1350 °C. In relation to activation energies, the values are close to that reported by Godoi and Souza [26] (0.50 eV) for LSM sintered at 1400 °C and higher than that measured by Tietz et al. [27] (0.10 eV) for LSM sintered at 1300 °C.

The two-probe method is not appropriate for a precise measurement, and it tends to include a large experimental error in the electric resistance owing to the electric resistance change at the electrodes. The four point probe is preferable over a two point probe because the contact and spreading resistances associated with the two point probe cannot be measured. This means that the true resistance cannot be accurately separated from the measured resistance. But two-point probe method is much easier to implement, especially for measurements at high temperatures. The two-probe method was adopted here because

Table 5
Conductivity of the sintered pellets at 600 and 1000 °C and activation energies.

Samples	Conductivity (S cm^{-1})		E_a (eV)
	600 °C	1000 °C	
$La_{0.8}Sr_{0.2}MnO_3$	2.1	6.0	0.67
$La_{0.7}Sr_{0.3}MnO_3$	2.0	6.8	0.78
$La_{0.6}Sr_{0.4}MnO_3$	1.5	7.5	0.87

of the simplicity; the conductivity values were valuable to indicate a tendency among the samples, not to obtain a real value.

4. Conclusions

$La_{0.7}Sr_{0.3}MnO_3$ powders were successfully synthesized by polymerizable complex method using citric acid (CA) and ethylene glycol (EG), varying the CA:metal ions molar ratio and calcination temperature. TGA analysis showed a large weight loss for the as-prepared samples due to decomposition of polymer network formed between CA and EG. XRD results showed that a minimum of CA:MI ratio of 3 is necessary for a single LSM phase formation, with good crystallization and nanometric crystallite sizes. The microstructure of the powder samples revealed by SEM analysis showed that the porosity is favored with increasing CA:metal ions ratio. In relation to calcination temperature, a pure LSM formation without secondary phases is obtained at 900 °C.

Using CA:metal ions ratio of 3 and calcination temperature at 900 °C, $La_{1-x}Sr_xMnO_3$ powders with different Sr content ($x = 0.2$–0.4) were synthesized. The powders presented LSM pure phase formation and BET surface areas of 4–10 $m^2\ g^{-1}$. The porosity of the pellets sintered at 1100 °C increased with Sr content, with values (40–52%) higher than those appropriate for application as cathode material in SOFCs. The electrical conductivity of the sintered pellets, measured by two-probe technique, increased with Sr content at 1000 °C, and the values were much lower than those measured by other techniques in the literature.

Acknowledgements

The authors thank Núcleo de Catálise (PEQ/COPPE/UFRJ) for BET analyses. The authors also acknowledge CNPq, CAPES and FAPERJ for financial support granted to carry out this work.

References

[1] S.C. Singhal, K. Kendall, High Temperature Solid Oxide Fuel Cells: Fundamentals Design and Applications, Elsevier Ltd., Oxford, 2004.
[2] N.Q. Minh, Ceramic fuel cells, J. Am. Ceram. Soc. 76 (1993) 563–588.
[3] T. Kawada, Perovskite oxide for cathode of SOFCs, in: T. Ishihara (Ed.), Perovskite Oxide for Solid Oxide Fuel Cells, Springer, New York, 2009, pp. 147–166.
[4] M. Gaudon, C. Laberty-Robert, F. Ansart, P. Stevens, A. Rousset, Preparation and characterization of $La_{1-x}Sr_xMnO_{3+\delta}$ ($0 \leq x \leq 0.6$) powder by sol–gel processing, Solid State Sci. 4 (2002) 125–133.
[5] Q. Zhang, T. Nakagawa, F. Saito, Mechanochemical synthesis of $La_{0.7}Sr_{0.3}MnO_3$ by grinding constituent oxides, J. Alloys Compd. 308 (2000) 121–125.
[6] L.A. Chick, L.R. Pederson, G.D. Maupin, J.L. Bates, L.E. Thomas, G.J. Exarhos, Glycine-nitrate combustion synthesis of oxide ceramic powders, Mater. Lett. 10 (1990) 6–12.
[7] L. Conceição, N.F.P. Ribeiro, J.G.M. Furtado, M.M.V.M. Souza, Effect of propellant on the combustion synthesized Sr-doped $LaMnO_3$ powders, Ceram. Int. 35 (2009) 1683–1687.
[8] R.J. Bell, G.J. Millar, J. Drennan, Influence of synthesis route on the catalytic properties of $La_{1-x}Sr_xMnO_3$, Solid State Ionics 131 (2000) 211–220.
[9] M. Kakihana, M. Arima, M. Yoshimura, N. Ikeda, Y. Sugitani, Synthesis of high surface area $LaMnO_{3+d}$ by a polymerizable complex method, J. Alloys Compd. 283 (1999) 102–105.
[10] W.-D. Yang, Y.-H. Chang, S.-H. Huang, Influence of molar ratio of citric acid to metal ions on preparation of $La_{0.67}Sr_{0.33}MnO_3$ materials via polymerizable complex process, J. Eur. Ceram. Soc. 25 (2005) 3611–3618.
[11] A. Gaki, O. Anagnostaki, D. Kioupis, T. Perraki, D. Gakis, G. Kakali, Optimization of $LaMO_3$ (M: Mn, Co, Fe) synthesis through the polymeric precursor route, J. Alloys Compd. 451 (2008) 305–308.
[12] M. Kakihana, 'Sol–gel' preparation of high temperature superconducting oxides, J. Sol-Gel Sci. Technol. 6 (1996) 7–55.
[13] M.P. Pechini, Method of preparing lead and alkaline-earth titanates and niobates and coating method using the same to form capacitors, US Patent no. 3330697, 1967.
[14] M. Popa, M. Kakihana, Synthesis of lanthanum cobaltite ($LaCoO_3$) by the polymerizable complex route, Solid State Ionics 151 (2002) 251–257.
[15] G.-J. Li, Z.-R. Sun, H. Zhao, C.-H. Chen, R.-M. Ren, Effect of temperature on the porosity, microstructure, and properties of porous $La_{0.8}Sr_{0.2}MnO_3$ cathode materials, Ceram. Int. 33 (2007) 1503–1507.
[16] G.K. Williamson, W.H. Hall, X-ray line broadening from filed aluminum and wolfram, Acta Metall. 1 (1953) 22–31.
[17] S. Biamino, C. Badini, Combustion synthesis of lanthanum chromite starting from water solutions: investigation of process mechanism by DTA–TGA–MS, J. Eur. Ceram. Soc. 24 (2004) 3021–3034.
[18] A. Ghosh, A.K. Sahu, A.K. Gulnar, A.K. Suri, Synthesis and characterization of lanthanum strontium manganite, Scripta Mater. 52 (2005) 1305–1309.
[19] Z. Gaoke, L. Ying, Y. Xia, W. Yanping, S. Ouyang, L. Hangxing, Comparison of synthesis methods, crystal structure and characterization of strontium cobaltite powder, Mater. Chem. Phys. 99 (2006) 88–95.
[20] M. Popa, J. Frantti, M. Kakihana, Characterization of $LaMeO_3$ (Me: Mn, Co, Fe) perovskite powders obtained by polymerizable complex method, Solid State Ionics 154–155 (2002) 135–141.
[21] D. Berger, V. Fruth, I. Jitaru, J. Schoonman, Synthesis and characterisation of $La_{1-x}Sr_xCoO_3$ with large surface area, Mater. Lett. 58 (2004) 2418–2422.
[22] R.V. Wandekar, B.N. Wani, S.R. Bharadwaj, Crystal structure, electrical conductivity, thermal expansion and compatibility studies of co-substituted lanthanum strontium manganite system, Solid State Sci. 11 (2009) 240–250.
[23] A Kumar, P.S. Devi, H.S. Maiti, Effect of metal ion concentration on synthesis and properties of $La_{0.84}Sr_{0.16}MnO_3$ cathode material, J. Power Sources 161 (2006) 79–86.
[24] C.C.T. Yang, W.C. Wei, A. Roosen, Electrical conductivity and microstructures of $La_{0.65}Sr_{0.3}MnO_3$–8 mol% yttria–stabilized zirconia, Mater. Chem. Phys. 81 (2003) 134–142.
[25] R.S. Guo, Q.T. Wei, H.L. Li, F.H. Wang, Synthesis and properties of $La_{0.7}Sr_{0.3}MnO_3$ cathode by gel combustion, Mater. Lett. 60 (2006) 261–265.
[26] G.S. Godoi, D.P.F. Souza, Electrical and microstructural characterization of $La_{0.7}Sr_{0.3}MnO_3$ (LSM), $Ce_{0.8}Y_{0.2}O_2$ (CY) and LSM-CY composites, Mater. Sci. Eng. B 140 (2007) 90–97.
[27] F. Tietz, I. Arul Raj, M. Zahid, D. Stöver, Electrical conductivity and thermal expansion of $La_{0.8}Sr_{0.2}(Mn,Fe,Co)O_{3-y}$ perovskites, Solid State Ionics 177 (2006) 1753–1756.